Correspondence to:
E. Douma,
emmadouma@gmail.com

Occurrence characteristics of relativistic electron microbursts from SAMPEX observations

Emma Douma[1] (ID), **Craig J. Rodger**[1] (ID), **Lauren W. Blum**[2] (ID), **and Mark A. Clilverd**[3] (ID)

[1]Department of Physics, University of Otago, Dunedin, New Zealand, [2]NASA Goddard Space Flight Center, Greenbelt, Maryland, USA, [3]British Antarctic Survey (NERC), Cambridge, UK

Abstract We study the occurrence of relativistic microbursts observed by the Solar Anomalous Magnetospheric Particle Explorer (SAMPEX) satellite. An algorithm is used to identify 193,694 relativistic microbursts in the > 1.05 MeV electron fluxes occurring across the time period 23 August 1996 to 11 August 2007, nearly a full solar cycle. Our observations are normalized to provide the change in absolute occurrence rates with various parameters. We find that relativistic microbursts are mostly confined to the outer radiation belt, from $L = 3-8$, occurring primarily on the morningside, between 0 and 13 magnetic local time (MLT). This L and MLT distribution is consistent with the L and MLT distribution of whistler mode chorus amplitude. Thus, our observations favor whistler mode chorus wave activity as a driver of relativistic microbursts. Relativistic microbursts become more frequent as the geomagnetic activity level increases and are more frequent during equinoxes than during the solstices. The peak occurrence frequency of the relativistic microbursts moves to lower L as the geomagnetic activity increases, reaching a peak occurrence rate of one microburst every 10.4 s (on average) at $L = 4$ for $6.6 \leq Kp \leq 8.7$. Microbursts primarily occur outside of the plasmapause and track the inward movement of the plasmapause with increasing geomagnetic activity. The L and MLT distribution of the relativistic microbursts exhibits a peak occurrence of one microburst every 8.6 (98.0) s during active (disturbed) conditions, with the peak located at $L = 5$ ($L = 5.5$) and 08 (08) MLT.

1. Introduction

Relativistic electron microbursts are intense short-duration (< 1 s) precipitation events of > 1 MeV electrons from the outer radiation belt into the atmosphere [*Blake et al.*, 1996]. Relativistic microburst precipitation events are believed to be significant contributors to radiation belt losses. It has been suggested that relativistic microbursts occurring during a single storm could empty the entire relativistic electron population [*Lorentzen et al.*, 2001a; *Clilverd et al.*, 2006; *Dietrich et al.*, 2010]. Thus, it is important to better understand the conditions under which relativistic microbursts occur, as well as the physical processes in space which drive this type of precipitation.

Many previous studies have been undertaken on relativistic microbursts using various satellites, most commonly using observations from the Solar Anomalous Magnetospheric Particle Explorer (SAMPEX) satellite. Additionally, an algorithm has been published in *O'Brien et al.* [2003] describing how to detect these relativistic microbursts in SAMPEX satellite data, which will be presented in detail below. Various other authors have used this algorithm including but not limited to *O'Brien et al.* [2004], *Johnston and Anderson* [2010], *Blum et al.* [2015], and *Kurita et al.* [2016]. However, the majority of relativistic microburst studies thus far have only considered relatively short time periods, ranging from a few case study storms [*Lorentzen et al.*, 2001a] to a few months of data [*Nakamura et al.*, 2000]. Studies using longer time periods have focused on particular storm types; for example, *Blum et al.* [2015] only considered high-speed stream (HSS)-driven storms. This is a deficiency we correct in the current study. We summarize below the primary conclusions regarding microburst occurrence which have appeared in the literature to date.

Relativistic microbursts are most often observed in the morning magnetic local time (MLT) sector, between midnight and noon [*Nakamura et al.*, 2000; *O'Brien et al.*, 2003; *Thorne et al.*, 2005; *Johnston and Anderson*, 2010; *Blum et al.*, 2015]. Furthermore, relativistic microbursts primarily occur in the $L = 3.5-6$ region [*Nakamura et al.*, 2000; *Blum et al.*, 2015] with the greatest frequency of occurrence at $L = 5$ [*O'Brien et al.*, 2003]. However, relativistic microbursts have been observed at comparatively large L (up to $L = 8$) [*Nakamura et al.*, 1995].

It is known that the occurrence of relativistic microbursts depends on the storm phase, with activity beginning at the onset of a geomagnetic storm and continuing well into the recovery phase [*Nakamura et al.*, 2000; *Lorentzen et al.*, 2001a; *O'Brien et al.*, 2003, 2004; *Johnston and Anderson*, 2010; *Comess et al.*, 2013; *Blum et al.*, 2015]. There is further evidence of this storm dependence through the relationship between relativistic microburst occurrence and geomagnetic indices. Relativistic microburst occurrence rates tend to increase during geomagnetically active periods [*Nakamura et al.*, 1995; *Comess et al.*, 2013] and correlate strongly with variations in both *Dst* and *Kp* [*Lorentzen et al.*, 2001a; *O'Brien et al.*, 2003; *Comess et al.*, 2013].

Additionally, the relativistic microburst MLT distribution evolves with geomagnetic activity level. During low *Kp* values the maximum occurrence of relativistic microbursts is located near MLT midnight, but, as the *Kp* values increase, the maximum moves toward MLT dawn [*Lorentzen et al.*, 2001b]. A similar evolution was reported by *O'Brien et al.* [2003] using the *Dst* index. The maximum occurrence of relativistic microbursts is located near MLT midnight for weak *Dst* activity and moves to the prenoon MLT sector for increased *Dst* activity [*O'Brien et al.*, 2003].

Relativistic microbursts occur primarily outside the plasmapause [*Lorentzen et al.*, 2001b; *O'Brien et al.*, 2003; *Johnston and Anderson*, 2010] and generally move to lower *L* during geomagnetic storms, following the inward radial movement of the plasmapause [*Nakamura et al.*, 1995, 2000; *Lorentzen et al.*, 2001a; *Johnston and Anderson*, 2010; *Blum et al.*, 2015].

It has been suggested for some time that relativistic microbursts are driven by pitch angle scattering of radiation belt electrons interacting with whistler mode chorus waves. However, at this stage there has been little direct experimental evidence to demonstrate this. Many studies in the current literature have concluded that their observations are consistent with chorus waves as the driver of relativistic microbursts. These arguments are based on an overlap, in both *L* and MLT space, of the active chorus regions with the microburst occurrence regions [*Nakamura et al.*, 2000; *Lorentzen et al.*, 2001b; *Johnston and Anderson*, 2010; *Kertsen et al.*, 2011; *Kurita et al.*, 2016] and the timescale of the chorus risers being comparable to the duration of the microbursts [*Nakamura et al.*, 2000; *Lorentzen et al.*, 2001b; *Kertsen et al.*, 2011]. Furthermore, modeling efforts show that chorus wave particle interactions at high magnetic latitudes (waves propagating away from the equator along the field line) can cause relativistic electron microbursts [*Thorne et al.*, 2005; *Saito et al.*, 2012; *Miyoshi et al.*, 2015], and the rising tone elements in chorus waves can reproduce the few hertz modulation of microbursts observed by SAMPEX [*Saito et al.*, 2012]. This relationship has led to the suggestion that observations of relativistic microbursts might be used as a proxy for chorus wave activity [*O'Brien et al.*, 2003], while noting that the microburst frequency drops off more rapidly than the chorus amplitude with increasing *L*. However, the absence of simultaneous < 100 keV precipitating electrons in both satellite and subionospheric observations during two relativistic microburst precipitation events fundamentally disagrees with the conclusion that whistler mode chorus waves are the drivers of the scattering [*Rodger et al.*, 2007].

Recently, a study was published by *Omura and Zhao* [2013] focused upon anomalous cyclotron resonance between relativistic electrons (> 1 MeV) and electromagnetic ion cyclotron (EMIC) triggered emissions. These authors reported that this resonance is effective, resulting in the efficient precipitation of relativistic electrons through nonlinear trapping by EMIC triggered emissions. *Omura and Zhao* [2013] conducted test particle simulations with a large number of relativistic electrons and found that in the presence of coherent EMIC triggered emissions with increasing frequencies the relativistic electrons at high pitch angles are guided to lower pitch angles resulting in relativistic microbursts. This comparatively new theoretical work indicates that there is uncertainty as to the dominant scattering process which leads to relativistic microbursts, suggesting that the occurrence of these precipitation events may need to be reexamined.

In this paper we use the *O'Brien et al.* [2003] method to produce a very large database of SAMPEX relativistic microburst detections that occurred across a long time period and over a broad range of geomagnetic conditions. By using this very large data set we can reliably correct for the sampling bias in the satellite observations. Hence, we can establish for the first time how the absolute relativistic microburst occurrence rate varies across multiple parameters. We discuss the distribution of the relativistic microbursts when projected onto the Earth's atmosphere and the influence of the Russell-McPherron effect. Additionally, we examine the *L* and MLT distribution of relativistic microbursts and, in particular, contrast the differences between various geomagnetic activity levels. Lastly, we compare the *L* and MLT distribution of relativistic microbursts to those of whistler mode chorus and EMIC waves, provided in the literature.

2. Experimental Data Set

The Solar Anomalous Magnetospheric Particle Explorer (SAMPEX) satellite was launched in July 1992, reentering the atmosphere in late 2012 [*Baker et al.*, 2012]. SAMPEX was in a low-altitude orbit (520–670 km) with an inclination of 82° [*Baker et al.*, 1993]. The altitude of SAMPEX satellite drops over the period analyzed. The SAMPEX data are available from the SAMPEX Data Center (http://www.srl.caltech.edu/sampex/DataCenter).

SAMPEX carried the Heavy Ion Large Telescope (HILT) instrument, which produced high sensitivity and high time resolution >1.05 MeV electron and >5 MeV proton flux measurements with an effective geometric factor of ~60 cm^2 sr [*Klecker et al.*, 1993]. The HILT instrument samples different pitch angles over different regions of the Earth but primarily samples the atmospheric loss cones [*Dietrich et al.*, 2010]. HILT is composed of a large area ion drift chamber, two position-sensitive proportional counters, an array of 16 silicon solid state detectors, and a CsI crystal unit [*Klecker et al.*, 1993]. In the current study we use row 4 of the solid state detector array as the temporal resolution of the sampling rate of this data set did not change over the lifetime of the satellite. Row 4 (SSD4) has a temporal resolution of 100 ms. All available HILT data at the SAMPEX Data Centre from 8 August 1996 through to the end of the data set on 3 November 2012 are included in our initial analysis.

The HILT instrument responds to both electron and protons; thus, as an initial processing step we remove all data coinciding with solar proton events. In order to define a solar proton event (SPE) we use the 5 min average >10 MeV proton flux measurements from the National Oceanic and Atmospheric Administration (NOAA) Geostationary Operational Environmental Satellites (GOES) spacecraft, available in the NASA High Resolution OMNI data set. The threshold level generally used by NOAA to define a SPE is the time when the proton flux is above 10 pfu (where pfu is the >10 MeV proton flux unit; i.e., protons s^{-1}sr^{-1}cm^{-2} at geostationary orbit). However, *Cresswell-Moorcock et al.* [2015] found that the *D* region of the upper atmosphere can respond to SPEs below the official threshold flux level, indicating that the official threshold may not remove all SPE contamination. Therefore, we have applied a more conservative threshold, such that a solar proton event is defined as the >10 MeV proton flux above 3 pfu in the 5 min GOES measurements.

As HILT responds to both protons and electrons we must also remove periods when SAMPEX was inside the South Atlantic Magnetic Anomaly (SAMA), where inner belt protons will reach SAMPEX altitudes. There is a flag in the data to indicate when SAMPEX is inside the SAMA; thus, any period where this flag variable had a value of 1 was removed from the analysis.

3. Event Selection

We apply the *O'Brien et al.* [2003] algorithm to row 4 of the HILT solid state detector array after the SPE removal. It was found that the algorithm did not correctly detect relativistic microbursts when SAMPEX was in a spinning mode. Thus, as part of further data processing we ensure that the satellite is not in the spin mode. There is another data flag, the attitude flag, which defines the quality of the data and also describes the mode of the satellite. Values in the attitude flag of 100 or 101 are an indication of high quality data from a spin mode, while values of 0 or 1 indicate high quality data from a nonspin mode. Thus, we only include in our analysis data that have an attitude flag value of 0 or 1.

We apply the *O'Brien et al.* [2003] algorithm to all the SAMPEX/HILT data from 23 August 1996 through to 3 November 2012 (after the removal of SPEs, SAMA regions, and times of spin mode). Unfortunately, the satellite was continuously in spin mode from late 2007 until reentry, limiting us to the period from 23 August 1996 through to 11 August 2007. The algorithm is as follows:

$$\frac{N_{100} - A_{500}}{\sqrt{1 + A_{500}}} > 10, \tag{1}$$

where N_{100} is the number of counts in 100 ms and A_{500} is the centered running average of N_{100} over five 100 ms intervals (i.e., over 500 ms). It should be noted that the algorithm does not perform well either at low radiation belt fluxes or during strong pitch angle diffusion [*O'Brien et al.*, 2003], which has been taken into account when interpreting the results presented later in this paper.

Figure 1 is an example of the microbursts detected by the algorithm on 17 August 1999 from 04:13:00 to 04:14:30 UT, where each red cross is a trigger in the algorithm identified as a relativistic microburst. There are
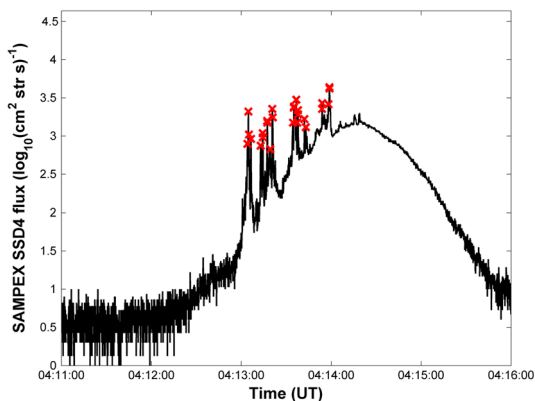
Figure 1. The SAMPEX > 1.05 MeV HILT electron flux on 17 August 1999, with each red cross indicating a trigger from the *O'Brien et al.* [2003] algorithm, identified as a relativistic microburst. Note the log scale of the fluxes.

27 microbursts detected by the algorithm in the time from 04:13:00 to 04:14:00 UT. It is common to get multiple triggers of relativistic microbursts over one pass through the radiation belt as relativistic microbursts are known to occur in trains of numerous bursts [*Lorentzen et al.*, 2001b].

We detect 193,694 relativistic electron microbursts between 23 August 1996 and 11 August 2007, after which SAMPEX was in spin mode. In the following sections we will discuss the absolute occurrence rates of relativistic microbursts. We have corrected the statistics presented below for any satellite sampling bias. We normalize the global microburst occurrence counts by the number of satellite samples in each latitude/longitude bin. We normalize the *L* and MLT distribution of relativistic microbursts by the number of satellite samples in each *L*/MLT bin.

4. Global Occurrence

The absolute occurrence rate of relativistic electron microbursts are distributed over the Earth as shown in Figure 2, which has been corrected for any satellite sampling bias. The resolution of Figure 2 is 2° in both latitude and longitude. The vast majority of the microbursts occur inside the region of the outer radiation belt, projected onto the Earth. The color bar in Figure 2 indicates the frequency with which we observe relativistic microbursts, which is slightly higher in the North Atlantic region and to the west of the Antarctic Peninsula. The relativistic microburst frequency is lower to the east of the Antarctic Peninsula. Comparing this to Figure 3 of *Dietrich et al.* [2010], the North Atlantic microburst occurrence frequency increase overlaps with the regions in which HILT measures only the bounce loss cone (BLC). Furthermore, part of the region where we note decreased relativistic microburst frequency corresponds to HILT sampling the trapped flux along with the BLC and the drift loss cone (DLC). Thus, we conclude that these differences in the relativistic microburst frequency over the Earth are a result of the HILT pitch angle sampling and the emptying of the loss cone in the longitudes of the Antarctic Peninsula.
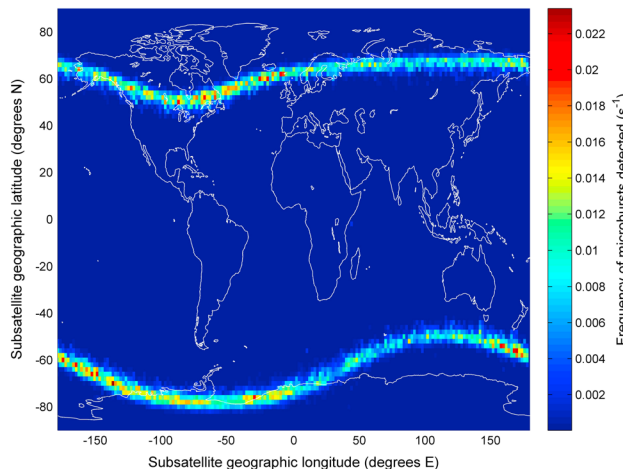

Figure 2. Frequency of occurrence of the relativistic microbursts identified between 1996 and 2007 projected onto the Earth.

5. Russell-McPherron Effect and Solar Cycle Dependence

The Russell-McPherron effect, outlined in *Russell and McPherron* [1973], explains the semiannual variation in geomagnetic activity occurring during both active and quiet geomagnetic conditions. The maximum activity occurs near the equinoxes (strong for inward (outward) interplanetary fields in the Northern Hemisphere spring (autumn)), while the minimum activity occurs near the solstices [*Russell and McPherron*, 1973; *Zhao and Zong*, 2012]. This is caused by a semiannual variation in the effective southward component of the interplanetary magnetic field (IMF), leading to the Earth extracting approximately 40% more energy from the solar
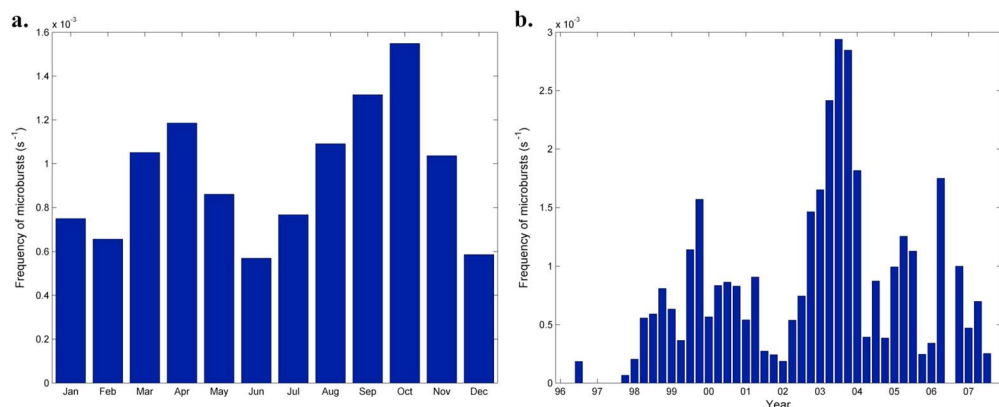
Figure 3. (a) The monthly distribution of microburst frequency from $L = 3-8$ and over all MLTs, displaying the Russell-McPherron effect. (b) The 3-monthly distribution of microburst frequency from $L = 3-8$ and over all MLT, displaying the solar cycle dependence.

wind during the equinoctial months than during the solstitial months [*Russell and McPherron*, 1973]. Both the maximums and the minimums in geomagnetic activity occur later during quiet years than during active years [*Russell and McPherron*, 1973]. Strong coupling during the equinoctial months is further limited by the spring-toward, fall-away rule [*Miyoshi and Kataoka*, 2008; *Kellerman et al.*, 2015], which influences the effectiveness of the solar wind driving inner magnetosphere activity. The spring-toward, fall-away conditions require the projection of the IMF geocentric solar ecliptic (GSE) y component to be "toward" (IMF azimuthal angle from the x axis ranges from 270° to 360°) during the months of Northern Hemisphere spring (February, March, April, and May) or "away" (IMF azimuthal angle from the x axis ranges from 90° to 180°) during the Northern Hemisphere autumn (August, September, October, and November) [*Miyoshi and Kataoka*, 2008]. Under these conditions there is an enhancement of the southward geocentric solar magnetic (GSM) IMF B_z component of the IMF such that the southward GSM B_z couples most efficiently to the Earth's magnetosphere. Under the opposite conditions (spring-away, fall-toward) there is a suppression of the southward IMF GSM B_z component reducing the efficiency of a southward GSM IMF B_z coupling to the Earth's magnetosphere [*Miyoshi and Kataoka*, 2008; *Kellerman et al.*, 2015].

A semiannual variation was also seen in relativistic electron fluxes by *McPherron et al.* [2009]. They found that if the IMF is predominantly northward, substorm activity will be at a minimum, allowing loss processes to dominate over acceleration of relativistic electrons [*McPherron et al.*, 2009]. In contrast, if IMF is predominantly southward, substorm activity will be stronger and persist for longer intervals, enhancing the internal processes that accelerate electrons [*McPherron et al.*, 2009; *Rodger et al.*, 2016] and control whistler mode chorus wave activity [*Miyoshi and Kataoka*, 2008; *Miyoshi et al.*, 2013]. Furthermore, *Baker et al.* [1999] reported that the equinoctial electron fluxes throughout the outer trapping zone are nearly a factor of 3 larger than the solstitial fluxes, consistent with the Russell-McPherron effect.

The Russell-McPherron effect can also be seen in the relativistic microbursts as shown in Figure 3a. The frequency of occurrence between $L = 3$ and 8 and over all MLTs maximizes in April and October (approximately the equinoctial months) and minimizes in June and December (approximately the solstitial months). The asymmetry seen in the size of the maximums is a result of only analyzing data inside one solar cycle; if we were able to average over multiple solar cycles, the maximums would be expected to be symmetric [*Russell and McPherron*, 1973].

Additionally, we investigate the IMF sector polarity associated with the microbursts. We use the spring-toward, fall-away rule outlined above as applied by *Miyoshi and Kataoka* [2008]. We undertook a superposed epoch analysis technique to investigate the B_z polarity around the time of the microbursts. We find that all our microburst events are associated with a southward B_z component. The IMF B_z has stronger values southward for microburst events which occur when there is less efficient coupling to the magnetosphere (spring-away, fall-toward) when compared with those which occur when there is more efficient coupling (spring-toward, fall-away). This is consistent with the Russell-McPherron effect as the IMF is offset northward at times of less efficient coupling to the magnetosphere (spring-away, fall-toward), requiring a larger southward B_z in order for the solar wind to couple to the magnetosphere and reconnection to occur.
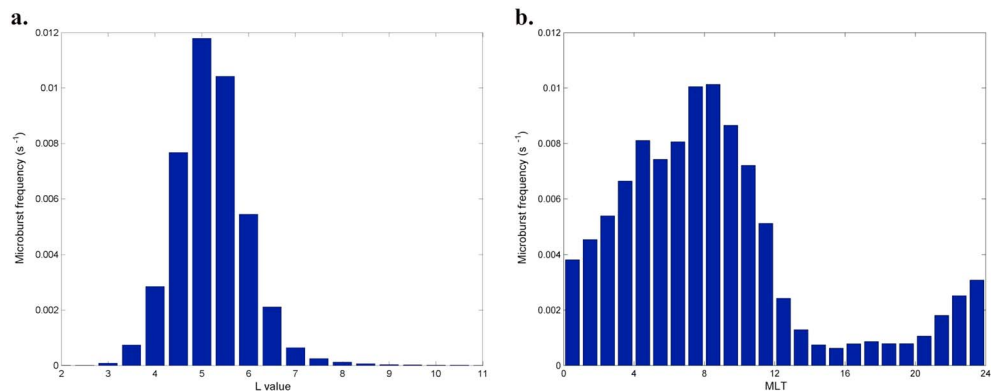
Figure 4. (a) The *L* distribution and (b) the MLT distribution of the frequency of occurrence of relativistic microbursts, corrected for satellite sampling bias.

We also consider how the relativistic microburst frequency is related to the solar cycle, as we have coverage of nearly an entire solar cycle (August 1996 to August 2007). Figure 3b presents the frequency of relativistic microbursts every 3 months for the entire temporal period. There is a clear peak in microburst frequency occurring in 2003 during the declining phase of solar cycle 23 and corresponding to the peak smoothed monthly average *Ap* values of solar cycle 23. There is also a peak between 1999 and 2000 which corresponds to the peak in the sunspot number of solar cycle 23. The year 2002 also corresponds to a peak in the sunspot number; however, we observe very little microbursts occurring during this year.

6. *L* and MLT Properties

The histogram of the relativistic microburst *L* values (corrected for satellite sampling bias), Figure 4a, indicates that these precipitation events are contained within $L = 3-8$, the expected location of the outer radiation belts. The peak in the occurrence frequency of the relativistic microbursts occurs at $L = 5$, at a rate of 0.012 microbursts s^{-1} (i.e., at $L = 5$ over all MLT, one microburst is detected, on average, every 83 s). The occurrence frequency drops more rapidly as one moves inward in *L* compared with outward in *L*. *Nakamura et al.* [2000] observed relativistic microburst events in similar *L* shells based on their observations of relativistic microbursts occurring in the Northern Hemisphere from September to December 1993. Both the upper and lower *L* values as well as the *L* value of peak microburst activity agrees with *O'Brien et al.* [2003], whose results are based on relativistic microbursts observations from 1996 to 2001 (recall that we extend this up to 2007 in the data set we analyze in the current study, so that it now includes the declining phase of the solar cycle as well).

The histogram of the occurrence with MLT (corrected for satellite sampling bias) in which we observe relativistic microbursts, Figure 4b, indicates that relativistic microbursts are more frequent on the morningside, from 0 to 13 MLT. The peak in occurrence frequency of relativistic microbursts occurs at 8 MLT, at a rate of 0.01 microbursts s^{-1} (i.e., one microburst is detected every 100 s). The occurrence frequency drops more rapidly for later MLT locations when compared to the change from the peak location toward earlier MLT locations. The occurrence frequency of relativistic microbursts minimizes at 15 MLT with a rate of 6×10^{-4} microbursts s^{-1} (i.e., one microburst detected every 28 min). The MLT morning sector peak in microburst occurrence has been well established in the literature using smaller data sets [e.g., *Nakamura et al.*, 2000; *O'Brien et al.*, 2003; *Blum et al.*, 2015], and our larger data set confirms the result. However, Figure 4b also indicates that there is a small population of relativistic microbursts occurring prior to midnight, from 20 to 24 MLT, with an occurrence rate at 23 MLT of 3×10^{-3} microbursts s^{-1}, i.e., one third of the peak morningside rate.

7. Geomagnetic Activity

The *L* distribution of relativistic microbursts is highly dependent on the level of geomagnetic activity. This variation is presented in Figure 5a with five geomagnetic activity levels, all corrected for the satellite sampling bias. During quiet geomagnetic conditions, $Kp \leq 3$ (the black line in Figure 5a), relativistic microbursts are very infrequent at all *L* values, with a peak occurrence of only 0.004 microbursts s^{-1} at $L = 5.5$. During disturbed geomagnetic conditions, $3 < Kp < 4.6$ (the blue line), relativistic microbursts become more frequent over the
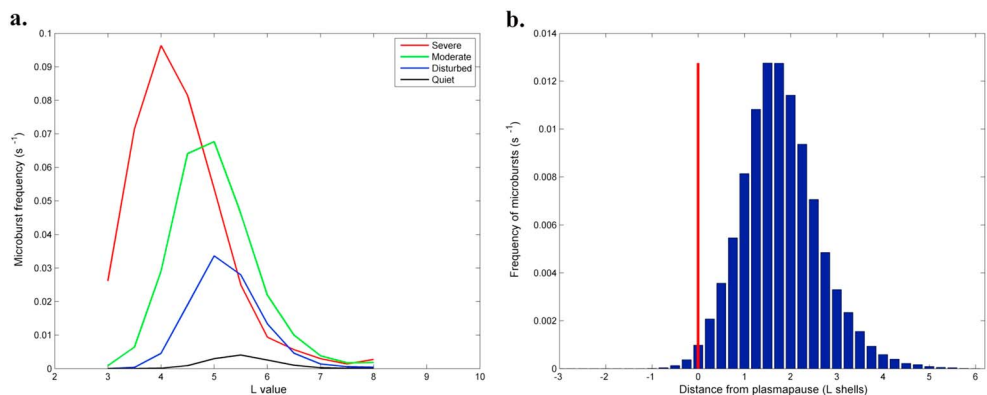
Figure 5. (a) The L distribution of the frequency of the relativistic microbursts for various geomagnetic activity levels. The black line indicates quiet conditions ($Kp \leq 3$), the blue line is associated with disturbed conditions ($3 < Kp < 4.6$), the green line is associated with moderate storms ($4.6 \leq Kp \leq 6.4$), and the red line is associated with severe storms ($6.6 \leq Kp \leq 8.7$). (b) The frequency of relativistic microbursts relative to the plasmapause. Here the red line indicates the modeled location of the plasmapause.

L values from 3 to 8 (recall that there is little microburst activity outside these L values), with a peak occurrence of 0.033 microbursts s^{-1} at $L = 5$. This trend continues, and as the geomagnetic activity level increases, the relativistic microbursts become more frequent over the range of L values at which relativistic microbursts are observed. During moderate conditions, $4.6 \leq Kp \leq 6.4$ (the green line), relativistic microbursts have a peak occurrence of 0.068 microbursts s^{-1} at $L = 5$. The relativistic microbursts become most frequent for severe geomagnetic conditions, $6.6 \leq Kp \leq 8.7$ (the red line), with a peak occurrence of 0.096 microbursts s^{-1} at $L = 4$. This peak relativistic microburst occurrence rate of 0.096 microbursts s^{-1} equates to an average of one microburst occurring every 10.4 s. Our data set does not contain any extreme geomagnetic conditions with $Kp > 8.7$.

Thus, we observe that the microbursts become more frequent as the geomagnetic activity level increases. Again, this agrees with previous studies of smaller data sets, in particular, with *O'Brien et al.* [2003], who found a similar relationship of relativistic microburst occurrence frequency with *Dst*, based on observations from 1996 to 2001. Additionally, we observe that the peak occurrence frequency of the relativistic microbursts moves to a lower L value; i.e., the microbursts move inward in L with increased geomagnetic activity. This is also seen in the literature based on smaller data sets [*Nakamura et al.*, 1995, 2000; *Lorentzen et al.*, 2001a; *Johnston and Anderson*, 2010; *Blum et al.*, 2015] and was described above.

To investigate how the relativistic microbursts relate to the plasmapause, we use the *O'Brien and Moldwin* [2003] Kp-based plasmapause model. The model is as follows:

$$L_{pp} = \left(-0.39 + 0.1326 \cos\left(\phi - \frac{8.3\pi}{6}\right)\right) \max\left[Kp_{(-36,-2)}\right] + \left(5.6 + 0.672 \cos\left(\phi - \frac{\pi}{4}\right)\right), \quad (2)$$

where $\max\left[Kp_{(-36,-2)}\right]$ is the maximum value of Kp taken from the previous 36 h to the previous 2 h and $\phi = 2\pi(\text{MLT}/24)$ [*O'Brien and Moldwin*, 2003]. The error of this model is given as 0.74 L in *O'Brien and Moldwin* [2003]. In Figure 5b we show the difference between the location of the relativistic microbursts and the location of the plasmapause in terms of L. Here a positive value corresponds to a location outside the plasmapause, and a negative value corresponds to inside the plasmasphere. The red line in Figure 5b indicates the location of the plasmapause. We can conclude that the relativistic microbursts almost always occur outside of the plasmapause with the highest occurrence frequency $\Delta L = 2$ beyond the plasmapause location. Given the uncertainty in the plasmasphere location model, we suggest that it is most likely that all microbursts occur outside the plasmapause.

The relativistic microbursts move inward in L with increased geomagnetic activity; however, they still remain outside of the plasmapause. Therefore, we conclude that the relativistic microbursts are tracking the inward movement of the plasmapause during enhanced geomagnetic activity. This tracking of the plasmapause has been reported earlier by *Johnston and Anderson* [2010] in the case study storms they considered.
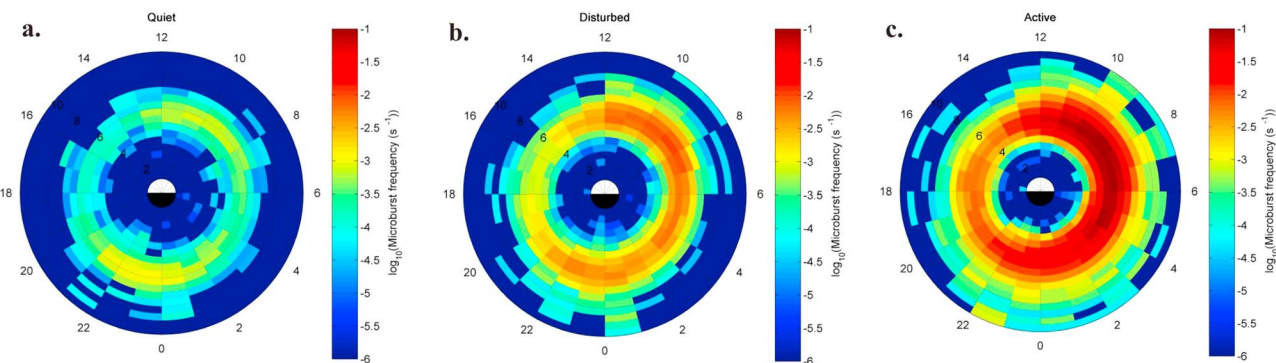
Figure 6. The *L* and MLT distribution of the frequency of relativistic microbursts during three levels of geomagnetic activity as measured by *AE**. (a) Quiet conditions, defined as $AE^* \leq 100$ nT, (b) disturbed conditions, defined as $100 < AE^* \leq 300$ nT, and (c) active conditions, defined as $AE^* > 300$ nT. Note that all three panels have the same log color scale.

Recall that the whistler mode chorus wave activity is observed outside the plasmapause [*Summers et al.*, 1998, 2007]. In contrast, EMIC waves have been observed both inside and outside of the plasmapause [*Meredith et al.*, 2003].

8. Comparison With Chorus and EMIC Occurrence Characteristics

As discussed above it is often thought that whistler mode chorus waves are driving the pitch angle scattering which lead to relativistic microbursts. However, recently there has been evidence published that EMIC waves could also produce relativistic microbursts. As a step toward answering which of the two waves are the dominant cause of relativistic microbursts, we compare the *L* and MLT distribution of the relativistic microbursts with those published in the literature for chorus and EMIC waves. Figure 6 presents the *L* and MLT distribution of the relativistic microbursts at three different levels of geomagnetic activity as measured by *AE**. Here we use the same definition of *AE** as used by *Li et al.* [2009], where *AE** is the mean of *AE* over the previous 1 h. The *L* and MLT distributions of the relativistic microbursts presented in Figure 6 have a resolution of 0.5 *L* and 1 h MLT. The colorbar describes the absolute frequency at which the relativistic microbursts occur on a log scale. In the following sections all ranges in MLT are described using a counterclockwise rotation in Figure 6.

8.1. Whistler Mode Chorus Comparison

Quiet geomagnetic conditions, $AE^* \leq 100$ nT, are presented in Figure 6a. It appears that there are two distinct peaks in the *L* and MLT distribution of relativistic microbursts. One peak occurs prior to midnight, with an occurrence rate of 1.2×10^{-3} microbursts s^{-1} at $L = 5.5$ and ~23 MLT, and the other occurs prior to noon, with an occurrence rate of 8.8×10^{-4} microbursts s^{-1} at $L = 5.5$ and ~10 MLT. These peaks are about 3 times larger than the rate midway between these points at $L = 5.5$ and ~4 MLT of $\approx 3 \times 10^{-4}$ microbursts s^{-1}. We compare the relativistic microburst occurrence distribution to the average root mean square chorus wave amplitudes presented in *Li et al.* [2009, Figure 2] and reproduced here as Figure 7. *Kertsen et al.* [2011] and *Cattell et al.* [2008] have shown that there is a relationship between large-amplitude whistler mode chorus and microbursts. *Li et al.* [2009] have presented the *L* and MLT distribution of whistler mode chorus for three categories of whistler mode amplitude, which has a very similar distribution to the figure presented here. Note that Figure 7 is the result of a statistical analysis of both lower amplitude chorus and large-amplitude chorus. Contrasting Figure 6 to Figure 7, we note that the equatorial chorus wave amplitude distribution for $AE^* \leq 100$ nT is highest in the dawn MLT sector (7–13 MLT). However, the strongest chorus wave activity is occurring at much higher *L* values than where relativistic microbursts occur in Figure 6a. Furthermore, there is no evidence of large-amplitude chorus waves in the region prior to midnight (21–24 MLT).

Relativistic microburst activity located near midnight during quiet geomagnetic conditions has been previously reported by *Lorentzen et al.* [2001b] (during low *Kp* values) and by *O'Brien et al.* [2003] (during weak *Dst* activity). Recall, however, that the *O'Brien et al.* [2003] algorithm does not perform well when radiation belt fluxes are low. Therefore, the distribution described above may not be representative of the relativistic microburst activity during quiet geomagnetic conditions and may be an artifact of the poor triggering rate of the algorithm at these times. Thus, we cannot make any firm conclusion about whether the relativistic microbursts occurring during quiet conditions are a result of scattering by whistler mode chorus waves.
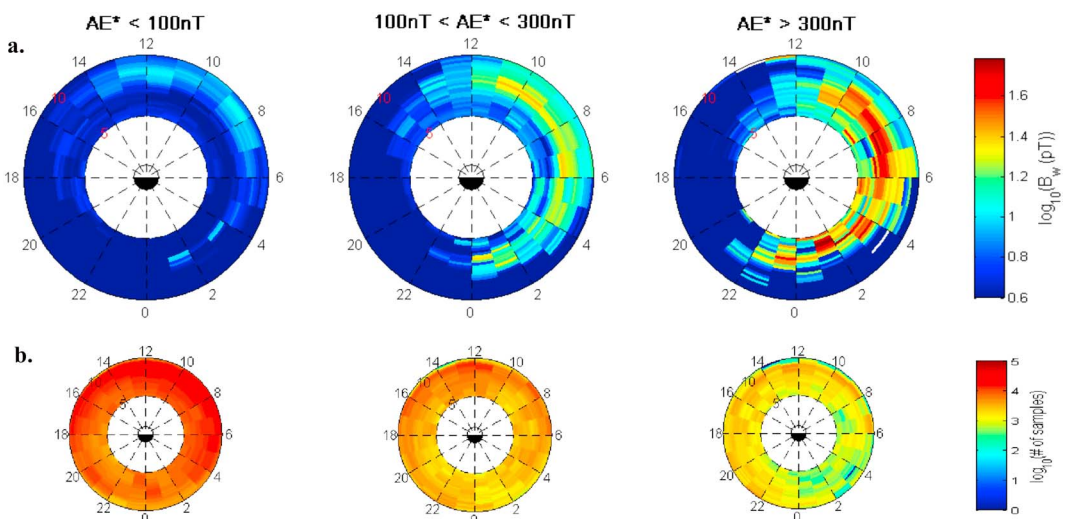
Figure 7. The global distribution of chorus adapted from *Li et al.* [2009, Figure 2]. The global distribution of chorus observed at the *L* shells between 5 and 10 categorized by different *AE** in the near equatorial (|MLAT| < 10°) regions. (a) The larger plots show RMS chorus wave amplitudes (pT), and (b) the smaller plots indicate the number of samples in each bin.

A modification of the algorithm and a reanalysis of the quiet time MLT distribution may resolve this uncertainty in future work.

Relativistic microburst distributions are presented in Figure 6b for disturbed conditions and Figure 6c for active conditions. During both disturbed, $100 < AE^* \leq 300$ nT, and active, $AE^* > 300$ nT, geomagnetic conditions we see that there is only one peak in the *L* and MLT distribution of relativistic microbursts. Furthermore, relativistic microbursts are frequent over a much larger continuous MLT range, beginning prior to midnight and continuing through until noon, i.e., from 21 MLT to 13 MLT. Relativistic microbursts are much more frequent during active geomagnetic conditions, with a peak occurrence rate of ~0.1 microbursts s^{-1} at $L = 5$ and from 6–10 MLT. In contrast, the peak occurrence rate for disturbed conditions is about 10 times lower with a value of ~0.01 microbursts s^{-1} at $L = 5.5$ and from 7–10 MLT.

To the best of our knowledge the *L*-MLT distribution of whistler mode chorus wave occurrence has not as yet been analyzed for different levels of geomagnetic activity. Thus, we will compare the relativistic microburst occurrence rates with the results of previous studies examining whistler mode chorus wave amplitudes. The equatorial whistler mode root mean square chorus wave amplitude distribution for active and disturbed conditions reported by *Li et al.* [2009, Figure 2] and reproduced here as Figure 7 has significant chorus activity at much lower *L* during disturbed and active geomagnetic conditions than that observed during quiet conditions. Further, stronger chorus wave amplitude is observed from MLT midnight through to noon (i.e., from 0 to 12 MLT) for disturbed conditions. During active conditions there is even stronger chorus wave amplitude observed prior to MLT midnight and through to postnoon (i.e., from 22 to 13 MLT). This strongly coincides with the relativistic microburst distributions we present in Figure 6. Therefore, we conclude that the majority of relativistic microburst activity is consistent with a whistler mode chorus wave driver, in agreement with the previous speculation in the literature described above.

We note that we have microbursts occurring in the region of 18 MLT where the chorus wave amplitude is < 4 pT. If it was only chorus waves driving the scattering resulting in microbursts, then chorus waves with amplitudes of < 4 pT should be able to scatter the relativistic electrons and drive microbursts. We point this out as a potential challenge to the modeling community.

8.2. EMIC Wave Comparison

We will not compare the EMIC distributions in *L* and MLT with the relativistic microburst occurrence during quiet conditions due to the algorithm limitations discussed above. Note that we find that the *L* and MLT distributions of the relativistic microbursts are indistinguishable when the geomagnetic activity is defined by either *AE* or *AE**, so we will compare to EMIC wave distributions using either of the geomagnetic activity indices.

Intense ($B_w^2 > 0.1$ nT^2) helium band EMIC waves are most prevalent in the afternoon sector (from 12 to 18 MLT) from $4 < L^* < 7$ during active conditions ($AE > 300$ nT) with an average percentage occurrence of 2.7% and an average intensity of 2 nT^2 [*Meredith et al.*, 2014]. Intense ($B_w^2 > 0.1$ nT^2) hydrogen band EMIC waves are also most prevalent in the same MLT and L region during active conditions, but they have a lower average percentage occurrence of 0.6% and a lower average intensity of 0.5 nT^2 [*Meredith et al.*, 2014]. Comparing this to our distribution of relativistic microbursts observed during active conditions, Figure 6c, we find significant relativistic microburst activity in the same MLT sector as the intense EMIC waves.

Rising or falling tone EMIC emissions, which occur in $> 30\%$ of all EMIC wave events, are observed mainly around noon (12 MLT) and do not appear to occur in the nightside MLT region [*Nakamura et al.*, 2016]. During low AE^* values ($AE^* < 300$ nT) rising and falling tone EMIC wave events are observed at $\sim$10 MLT, while under higher AE^* values ($AE^* > 300$ nT) they are observed at $\sim$15 MLT over $L = 5$–10 [*Nakamura et al.*, 2016]. Comparing this to our distribution of relativistic microburst occurrence rate during active conditions, Figure 6c, we observe that the reported peak in EMIC rising/falling tone emissions for lower AE^* values coincides with our peak region of relativistic microburst occurrence. During more active AE^* conditions the MLT and L region of peak EMIC rising/falling tone emissions no longer coincide with the peak relativistic microburst occurrence, although we do observe less frequent microbursts at $\sim$15 MLT. It appears that reported occurrence properties of EMIC rising/falling tone emissions are unable to account for the relativistic microbursts occurring in the nightside MLT region.

Overall EMIC waves are most often observed in the dayside outer magnetosphere with occurrence rates reaching $\sim$10% during intervals of moderate ($100 < AE < 300$ nT) and enhanced ($AE > 300$ nT) substorm activity [*Usanova et al.*, 2012]. During moderate geomagnetic conditions ($100 < AE < 300$ nT) the peak occurrence of EMIC waves is at 8–17 MLT at $L \geq 4$ [*Saikin et al.*, 2016], while during active conditions ($AE > 300$ nT) the peak occurrence of EMIC waves is in the afternoon MLT sector (12–18 MLT) from $L = 4$ to 6 with an occurrence rate of $\sim$25% [*Usanova et al.*, 2012; *Saikin et al.*, 2016]. More recently, EMIC waves have also been observed in the dusk MLT sector (from 18 to 24 MLT) with occurrence rates increasing with geomagnetic activity [*Saikin et al.*, 2016]. That study found that the average occurrence rate of EMIC waves in this MLT sector reaches $\sim$15% over $L = 4$–6 during active geomagnetic conditions [*Saikin et al.*, 2016]. Comparing this to the L and MLT distribution of relativistic microbursts, we note some similarities in the distributions. The EMIC activity observed during both moderate and active geomagnetic conditions from 8 to 17 MLT is coincident in L with the relativistic microburst activity along with the EMIC activity observed in the dusk sector, from 18 to 24 MLT. However, the frequent relativistic microburst activity from 24 to 8 MLT does not coincide with that seen in the patterns of EMIC activity. Therefore, only some of the relativistic microburst activity is consistent with an EMIC wave driver.

EMIC waves might be the cause of the smaller population of precipitation events seen in the MLT region from 13 to 22 MLT, where chorus amplitudes are very low [*Li et al.*, 2009, Figure 2].

9. Summary and Conclusions

We have applied the *O'Brien et al.* [2003] algorithm to row 4 of the HILT instrument on board the SAMPEX satellite from 1996 to 2012, excluding periods of SPE, satellite spin, and regions within the SAMA. From this we identify 193,694 relativistic microbursts in the > 1.05 MeV electron fluxes occurring across the time period from 23 August 1996 through to 11 August 2007.

From this large data set of events we find that relativistic microbursts are largely confined to the outer radiation belt, from $L = 3$ to 8. Furthermore, they occur primarily on the morningside, between 0 and 13 MLT. Additionally, the Russell-McPherron effect is observed. Relativistic microbursts become more frequent as the geomagnetic activity level increases as measured by either Kp or AE^*, with microbursts being most frequent during active geomagnetic conditions. The peak occurrence frequency of the relativistic microbursts moves inward (to lower L) as the geomagnetic activity increases, to reach a peak occurrence rate of one microburst every 10.4 s at $L = 4$ for $6.6 \leq Kp \leq 8.7$. Microbursts primarily occur outside of the plasmapause. We suggest that the relativistic microbursts track the inward movement of the plasmapause as geomagnetic activity increases.

During quiet geomagnetic conditions, as measured by AE^*, the L and MLT distribution of relativistic microbursts appears to have two distinct occurrence rate peaks. One of these is located prior to MLT midnight, with a peak occurrence rate of one microburst every 13.8 min at $L = 5.5$ and $\sim$23 MLT and the other occurring

prior to noon, with a peak occurrence rate of one microburst every 18.9 min at $L = 5.5$ and $\sim$10 MLT. However, due to the poor triggering rate of the algorithm under these conditions, we cannot conclude whether these relativistic microbursts are a result of scattering by whistler mode chorus, EMIC waves, or some other source.

During disturbed and active geomagnetic conditions, as measured by AE^*, the L and MLT distribution of the relativistic microbursts has only one peak occurrence location, with an occurrence of one microburst every 8.6 (98.0) s during active (disturbed) conditions at $L = 5$ ($L = 5.5$) and 08 (08) MLT. Whistler mode chorus waves have large amplitudes in the MLT region from 22 to 13 MLT coincident in L with the relativistic microburst activity. EMIC wave occurrence is most frequent from 8 to 17 MLT during both moderate and active conditions and from 18 to 24 MLT during active conditions, indicating some coincidence in L with the relativistic microburst activity.

The relativistic microbursts occurring from 22 to 13 MLT are consistent with scattering by whistler mode chorus waves. In contrast, relativistic microbursts in the 8–17 MLT region are consistent with scattering by EMIC waves. There are two regions of overlap from 8 to 13 MLT and from 22 to 24 MLT where the relativistic microbursts are consistent with scattering by either whistler mode chorus waves or EMIC waves. However, as relativistic microbursts are far more frequent in the 22–13 MLT region than other MLT regions, our observations favor whistler mode chorus wave activity as the primary driver of relativistic microbursts during geomagnetically active periods.

Finally, we caution that correlation does not imply causation, and care must be taken in conclusions drawn from comparisons of the overall L and MLT distributions. Our study provides more suggestive evidence toward the potential linkages between these waves and the relativistic electron microbursts, as has been suggested by theory. As yet a direct one to one linkage between such waves, in situ scattering, and these microbursts is lacking from the literature.

References

Baker, D. N., G. M. Mason, O. Figueroa, G. Colon, J. G. Watzin, and R. M. Aleman (1993), An overview of the Solar, Anomalous, and Magnetospheric Particle Explorer (SAMPEX) mission, *IEEE Trans. Geosci. Remote Sens.*, 31, 531–541, doi:10.1109/36.225519.

Baker, D. N., S. G. Kanekal, T. I. Pulkkinen, and J. B. Blake (1999), Equinoctial and solstitial averages of magnetospheric relativistic electrons: A strong semiannual modulation, *Geophys. Res. Lett.*, 26, 3193–3196, doi:10.1029/1999GL003638.

Baker, D. N., J. E. Mazur, and G. Mason (2012), SAMPEX to reenter atmosphere: Twenty-year mission will end, *Space Weather*, 10, S05006, doi:10.1029/2012SW000804.

Blake, J. B., M. D. Looper, D. N. Baker, R. Nakamura, B. Klecker, and D. Hovestadt (1996), New high temporal and spatial resolution measurements by SAMPEX of the precipitation of relativistic electrons, *Adv. Space Res.*, 18, 171–186, doi:10.1016/0273-1177(95)00969-8.

Blum, L., X. Li, and M. Denton (2015), Rapid MeV electron precipitation as observed by SAMPEX/HILT during high-speed stream-driven storms, *J. Geophys. Res. Space Physics*, 120, 3783–3794, doi:10.1002/2014JA020633.

Cattell, C., et al. (2008), Discovery of very large amplitude whistler-mode waves in Earth's radiation belts, *Geophys. Res. Lett.*, 35, L01105, doi:10.1029/2007GL032009.

Clilverd, M. A., C. J. Rodger, and T. Ulich (2006), The importance of atmospheric precipitation in storm-time relativistic electron flux drop outs, *Geophys. Res. Lett.*, 33, L01102, doi:10.1029/2005GL024661.

Comess, M. D., D. M. Smith, R. S. Selesnick, R. M. Millan, and J. G. Sample (2013), Duskside relativistic electron precipitation as measured by SAMPEX: A statistical survey, *J. Geophys. Res. Space Physics*, 118, 5050–5058, doi:10.1002/jgra.50481.

Cresswell-Moorcock, K., C. J. Rodger, M. A. Clilverd, and D. K. Milling (2015), Techniques to determine the quiet day curve for a long period of subionospheric VLF observations, *Radio Sci.*, 50, 453–468, doi:10.1002/2015RS005652.

Dietrich, S., C. J. Rodger, M. A. Clilverd, J. Bortnik, and T. Raita (2010), Relativistic microburst storm characteristics: Combined satellite and ground-based observations, *J. Geophys. Res.*, 115, A12240, doi:10.1029/2010JA015777.

Johnston, W. R., and P. C. Anderson (2010), Storm time occurrence of relativistic electron microbursts in relation to the plasmapause, *J. Geophys. Res.*, 115, A02205, doi:10.1029/2009JA014328.

Kellerman, A. C., R. L. McPherron, and J. M. Weygand (2015), On the azimuthal evolution and geoeffectiveness of the SIR-associated stream interface, *J. Geophys. Res. Space Physics*, 120, 1489–1508, doi:10.1002/2014JA020334.

Kertsen, K., C. A. Cattell, A. Breneman, K. Goetz, P. J. Kellogg, J. R. Wygant, L. B. Wilson III, J. B. Blake, M. D. Looper, and I. Roth (2011), Observation of relativistic electron microbursts in conjunction with intense radiation belt whistler-mode waves, *Geophys. Res. Lett.*, 38, L08107, doi:10.1029/2011GL046810.

Klecker, B., et al. (1993), HILT: A heavy ion large area proportional counter telescope for solar and anomalous cosmic rays, *IEEE Trans. Geosci. Remote Sens.*, 31, 542–548, doi:10.1109/36.225520.

Kurita, S., Y. Miyoshi, J. B. Blake, G. D. Reeves, and C. A. Kletzing (2016), Relativistic electron microbursts and variations in trapped MeV electron fluxes during the 8–9 October 2012 storm: SAMPEX and Van Allen Probes observations, *Geophys. Res. Lett.*, 43, 3017–3025, doi:10.1002/2016GL068260.

Li, W., R. M. Thorne, V. Angelopoulos, J. Bortnik, C. M. Cully, B. Ni, O. LeContel, A. Roux, U. Auster, and W. Magnes (2009), Global distribution of whistler-mode chorus waves observed on the THEMIS spacecraft, *Geophys. Res. Lett.*, 36, L09104, doi:10.1029/2009GL037595.

Lorentzen, K. R., M. D. Looper, and J. B. Blake (2001a), Relativistic electron microbursts during the GEM storms, *Geophys. Res. Lett.*, 28, 2573–2576, doi:10.1002/jgra.50477.

Lorentzen, K. R., J. B. Blake, U. S. Inan, and J. Bortnik (2001b), Observations of relativistic electron microbursts in association with VLF chorus, *J. Geophys. Res.*, 106, 6017–6027, doi:10.1029/2000JA003018.

McPherron, R. L., D. N. Baker, and N. U. Crooker (2009), Role of the Russell-McPherron effect in the acceleration of relativistic electrons, _J. Atmos. Sol. Terr. Phys._, _71_, 1032–1044, doi:10.1016/j.jastp.2008.11.002.

Meredith, N. P., R. M. Thorne, R. B. Horne, D. Summers, B. J. Fraser, and R. R. Anderson (2003), Statistical analysis of relativistic electron energies for cyclotron resonance with EMIC waves observed on CRRES, _J. Geophys. Res._, _108_(A6), 1250, doi:10.1029/2002JA009700.

Meredith, N. P., R. B. Horne, T. Kersten, B. J. Fraser, and R. S. Grew (2014), Global morphology and spectral properties of EMIC waves derived from CRRES observations, _J. Geophys. Res. Space Physics_, _119_, 5328–5342, doi:10.1002/2014JA020064.

Miyoshi, Y., and R. Kataoka (2008), Flux enhancement of the outer radiation belt electrons after the arrival of stream interaction regions, _J. Geophys. Res._, _113_, A03S09, doi:10.1029/2007JA012506.

Miyoshi, Y., R. Kataoka, Y. Kasahara, A. Kumamoto, T. Nagai, and M. Thomsen (2013), High-speed solar wind with southward interplanetary magnetic field causes relativistic electron flux enhancement of the outer radiation belt via enhanced condition of whistler waves, _Geophys. Res. Lett._, _40_, 4520–4525, doi:10.1002/grl.50916.

Miyoshi, Y., et al. (2015), Energetic electron precipitation associated with pulsating aurora: EISCAT and Van Allen Probes observations, _J. Geophys. Res. Space Physics_, _120_, 2754–2766, doi:10.1002/2014JA020690.

Nakamura, R., D. N. Baker, J. B. Blake, S. Kanekal, B. Klecker, and D. Hovestadt (1995), Relativistic electron precipitation enhancements near the outer edge of the radiation belt, _Geophys. Res. Lett._, _22_, 1129–1132, doi:10.1029/95GL00378.

Nakamura, R., M. Isowa, Y. Kamide, D. N. Baker, J. B. Blake, and M. Looper (2000), SAMPEX observations of precipitation bursts in the outer radiation belt, _J. Geophys. Res._, _105_, 15,875–15,885, doi:10.1029/2000JA900018.

Nakamura, S., Y. Omura, and V. Angelopoulos (2016), A statistical study of EMIC rising and falling tone emissions observed by THEMIS, _J. Geophys. Res. Space Physics_, _121_, 8374–8391, doi:10.1002/2016JA022353.

O'Brien, T. P., K. R. Lorentzen, I. R. Mann, N. P. Meredith, J. B. Blake, J. F. Fennell, M. D. Looper, D. K. Milling, and R. R. Anderson (2003), Energization of relativistic electrons in the presence of ULF wave power and MeV microbursts: Evidence for dual ULF and VLF acceleration, _J. Geophys. Res._, _108_(A8), 1329, doi:10.1029/2002JA009784.

O'Brien, T. P., and M. B. Moldwin (2003), Empirical plasmapause models from magnetic indices, _Geophys. Res. Lett._, _30_, 1152, doi:10.1029/2002GL016007.

O'Brien, T. P., M. D. Looper, and J. B. Blake (2004), Quantification of relativistic electron microburst losses during the GEM storms, _Geophys. Res. Lett._, _31_, L04802, doi:10.1029/2003GL018621.

Omura, Y., and Q. Zhao (2013), Relativistic electron microbursts due to nonlinear pitch angle scattering by EMIC triggered emissions, _J. Geophys. Res. Space Physics_, _118_, 5008–5020, doi:10.1002/jgra.50477.

Rodger, C. J., M. A. Clilverd, D. Nunn, P. T. Verronen, J. Bortnik, and E. Turunen (2007), Storm time, short-lived bursts of relativistic electron precipitation detected by subionospheric radio wave propagation, _J. Geophys. Res._, _112_, A07301, doi:10.1029/2007JA012347.

Rodger, C. J., K. Cresswell-Moorcock, and M. A. Clilverd (2016), Nature's grand experiment: Linkage between magnetospheric convection and the radiation belts, _J. Geophys. Res. Space Physics_, _121_, 171–189, doi:10.1002/2015JA021537.

Russell, C. T., and R. L. McPherron (1973), Semiannual variation of geomagnetic activity, _J. Geophys. Res._, _78_, 92–108, doi:10.1029/JA078i001p00092.

Saikin, A. A., J.-C. Zhang, C. W. Smith, H. E. Spence, R. B. Torbert, and C. A. Kletzing (2016), The dependence on geomagnetic conditions and solar wind dynamic pressure of the spatial distributions of EMIC waves observed by the Van Allen Probes, _J. Geophys. Res. Space Physics_, _121_, 4362–4377, doi:10.1002/2016JA022523.

Saito, S., Y. Miyoshi, and K. Seki (2012), Relativistic electron microbursts associated with whistler chorus rising tone elements: GEMSIS-RBW simulations, _J. Geophys. Res._, _117_, A10206, doi:10.1029/2012JA018020.

Summers, D., R. M. Thorne, and F. Xiao (1998), Relativistic theory of wave-particle resonant diffusion with application to electron acceleration in the magnetosphere, _J. Geophys. Res._, _103_, 20,487–20,500, doi:10.1029/98JA01740.

Summers, D., B. Ni, and N. P. Meredith (2007), Timescales for radiation belt electron acceleration and loss due to resonant wave-particle interactions: 2. Evaluation for VLF chorus, ELF hiss and electromagnetic ion cyclotron waves, _J. Geophys. Res._, _112_, A04207, doi:10.1029/2006JA011801.

Thorne, R. M., T. P. O'Brien, Y. Y. Shprits, D. Summers, and R. B. Horne (2005), Timescale for MeV electron microburst loss during geomagnetic storms, _J. Geophys. Res._, _110_, A09202, doi:10.1029/2004JA010882.

Usanova, M. E., I. R. Mann, J. Bortnik, L. Shao, and V. Angelopoulos (2012), THEMIS observations of electromagnetic ion cyclotron wave occurrence: Dependence on _AE_, _SYMH_, and solar wind dynamic pressure, _J. Geophys. Res._, _117_, A10218, doi:10.1029/2012JA018049.

Zhao, H., and Q.-G. Zong (2012), Seasonal and diurnal variation of geomagnetic activity: Russell-McPherron effect during different IMF polarity and/or extreme solar wind conditions, _J. Geophys. Res._, _117_, A11222, doi:10.1029/2012JA017845.